EFFECT OF OPERATING CONDITIONS ON THE PERFORMANCE OF THE BUBBLE PUMP OF ABSORPTION-DIFFUSION REFRIGERATION CYCLES

by

Ali BENHMIDENE [a*], ***Bechir CHAOUACHI*** [a], ***Mahmoud BOUROUIS*** [b], ***and Slimane GABSI*** [a]

[a] Research Unit Environment, Catalysis and Process Analysis URECAP
The National School of Engineering of Gabes, Gabes, Tunisia
[b] Department of Mechanical Engineering, Universitat Rovira i Virgili, Tarragona, Spain

Original scientific paper
UDC: 621.564.2:66.08
DOI: 10.2298/TSCI100601002B

The mathematical model will be able to predict the operated condition (required tube diameters, heat input. and submergence ratio….). That will result in a successful bubble pump design and hence a refrigeration unit In the present work a one-dimensional two-fluid model of boiling mixing ammonia-water under constant heat flux is developed. The present model is used to predict the outlet liquid and vapor velocities and pumping ratio for different heat flux input to pump. The influence of operated conditions such as: ammonia fraction in inlet solution and tube diameter on the functioning of the bubble pump is presented and discussed. It was found that, the liquid velocity and pumping ratio increase with increasing heat flux, and then it decreases. Optimal heat flux depends namely on tube diameter variations. Vapor velocity increases linearly with increasing heat flux under designed conditions.

Keys words: *bubble pump, two-fluid model, simulation, heat flux, operating conditions*

Introduction

A diffusion-absorption refrigeration cycle or a pumpless vapor absorption refrigeration cycle holds a great significance in noiseless refrigeration applications. The diffusion-absorption cycle relies on a bubble pump to pump the solution from the absorber to the boiler [1, 2]. A bubble pump is a fluid pump that operates on thermal energy to pump liquid from lower level to the higher level.

Heat applied to the pump causes formation of bubbles and the density of strong solution in the vertical pump tube is reduced so that the solution is forced to the top by the static head of solution in the absorber vessel. The vapor which is released by boiling the solution will eventually become the condensed refrigerant, and its mass rate will dictate the refrigeration capacity of the refrigerator. According to established theory of absorption

* Corresponding author; e-mail: aahmiden@yahoo.fr

refrigeration, this mass rate of refrigerant is supported by the circulation rates of the strong and week solutions and their concentration difference [3].

The experiments and theoretical considerations showed that, for a specific heat input, the diameter of the lift tube has no effect on the pumping rate if the pump is running in the slug or churn flow regimes [4, 5]. When the maximum lift-tube diameter is exceeded, the flow pattern changes from slug flow to an intermittent churn-type flow [5, 6]. After a certain pumping height is exceeded, the pumping action stopped.

Pfaff *et al*. [7] studied the bubble pump with a lithium bromide-water vapor absorption cycle. They developed a mathematical model using the manometer principle to evaluate the bubble pump performance. They found that the pumping ratio is independent of the heat input. However, the frequency of the pumping action increases as the heat inputs to the bubble pump increases, or if the tube diameter decreases. The model was then used to analyze an ammonia-water system and it was found that the diameter that maximizes the efficiency of the bubble pump is between 4 mm and 26 mm for a liquid pumping rate between 0.0025 kg/s and 0.02 kg/s. However, the efficiency rapidly decreases when diameters below the optimum values are used; therefore it is recommended that the diameter should be slightly larger than the optimum value.

To increase its refrigeration capacity, a multiple lift-tube bubble pump can be used, in order to increase the volume flow rates of the fluids, which are directly related to the amount of refrigerant produced. Vicatos *et al.* [3] testing on a diffusion-absorption plant using a multiple lift tube bubble pump, and the effects of additional tubes on the system's performance have been recorded. Although a full range of heat inputs could not be implemented, because of the limitations of the components of the unit itself, it was observed that the refrigeration cooling capacity was increased without a significant drop in coefficient of performance (COP). It was concluded that the multiple lift tube bubble pump has no limitation to the fluid flow rate and depends solely on the amount of heat input. This gives the freedom to design the lift tube pump according to the refrigeration demand of the unit, and not the other way round which is the current approach by the manufacturers world wide.

The bubble pump model presented by Delano [8] assumed that all flow takes place in the slug flow regime. At first, it may seem that a pump tube with a larger diameter would always be advantageous. However, increasing the diameter when the liquid flow is constant will eventually cause the assumed slug flow to change to bubbly flow. Delano concluded that increasing the heat input to the bubble pump for a fixed submergence ratio increases the flow rate of the liquid through the bubble pump to a maximum and any further increase in the heat input decreases the liquid flow rate. White [9] showed a rapid decrease in efficiency when the diameter drops below a particular value. A numerical and experimental study of convective boiling of a binary organic solution in a vertical tube was conducted by Levy *et al.* [10]. They obtained a detailed description of the flow characteristics. The influence of the heat source and operating pressure on the flow characteristics was examined both numerically and experimentally. Jakob *et al*. [11] reported that the indirectly heated generator with its bubble pump is the main new feature of a solar heat driven ammonia-water diffusion-absorption cooling machine and that all the prototypes constructed performed well. The performance of three diffusion absorption refrigeration (DAR) systems, which differ in their generator and bubble pump configuration, was studied numerically by Zohar *et al.* [12]. They showed that the configuration that integrated both the generator and the bubble pump is of great interest. An experimental investigation of an air-cooled diffusion-absorption machine operating with a binary light hydrocarbon mixture (C_4H_{10}/C_9H_{20}) as working fluids and helium as pressure

equalizing inert gas is presented by Ben Ezzine *et al*. [13]. The experimental results show that the bubble pump exiting temperature as well as those of the major components of the machine but the absorber is very sensitive to the heat power inputs to the bubble pump. For bubble pump heat inputs from 170 to 350 W, the driving temperature varies in the range of 120-150 °C.

Except of Levy *et al*. [10], most of the models reported in the literature for two--phase flow in a bubble pump, use the Beattie and Whalley's method [14] and the drift flux method (Zuber and Findlay [15]) to calculate the two-phase friction factor and the gas void fraction, respectively. The difference between these models is the value of the coefficients used in the drift flux model.

In the recent decades, significant developments in the two-phase flow formulation have been accomplished by introducing and improving the two-fluid model. The two-fluid model can be considered the most detailed and accurate macroscopic formulation of the thermo-fluid dynamics of two-phase flow [10, 16-18]. This model treats the general case of modeling each phase or component as a separate fluid with its own set of governing balance equations.

In the present study, the bubble pump was a vertical uniformly heated tube with an ammonia-water mixture. A numerical study based on two-fluid model was carried out to investigate the influence of heat flux input in the bubble pump, for different operating conditions such as tube diameter, ammonia fraction in solution and inlet pressure on the optimum heat flux input in the bubble pump.

Mathematical modeling

The diffusion-absorption refrigeration cycle consists of a generator bubble pump, an absorber, an evaporator and a condenser, and usually operates with ammonia/water/hydrogen or helium as working fluid. Figure 1 shows the main components of an absorption-diffusion refrigeration cycle and flow configurations in the bubble pump [19].

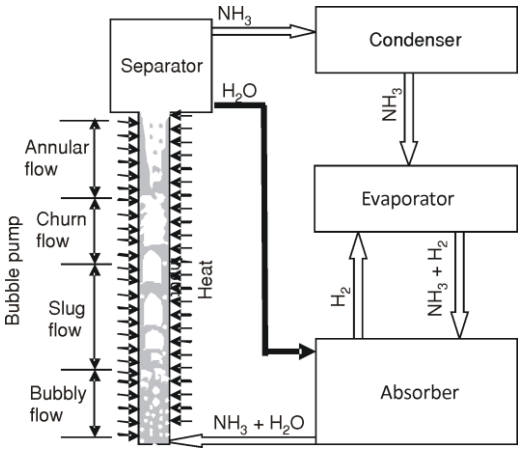

Figure 1. Main components of an absorption--diffusion refrigeration cycle and flow configurations in the bubble pump

In the diffusion-absorption cycle, the bubble pump is a heated tube that lifts fluid from a lower reservoir to a higher one (fig. 1). The generator configuration is of great importance. Heat is usually supplied at the bottom of the tube [3, 7, 9]. In the present work, heat is applied along all the tube length. This configuration of the bubble pump has two advantageous. First, it increases the COP of the cycle using minimum heat as possible and desorbing as much refrigerant as possible [12]. Second, it can be heated using solar thermal energy by integrating the bubble pump tubes and the solar collector [11, 20, 21].

In the present work, the two-fluid model was used for the two-phase flow region considering the hydrodynamic non-equilibrium between the liquid and vapor phases. The

flow configuration was not limited to the slug regime [8, 9], starting as bubbly and ending as annular (fig. 1).

The two-fluid model

The liquid and vapor superficial velocities and the void fraction throughout the tube are predicted using a 1-D two-fluid model**.** In the two-phase region, the general conservation equations of mass, momentum, and energy were formulated by Ishii *et al*. [22]. For the steady-state with negligible kinetic and potential energy, the conservation equations are reduced to the following equations:

– phase mass equations

$$\frac{\mathrm{d}}{\mathrm{d}z}\ \alpha\rho_{\mathrm{G}}u_{\mathrm{G}}\ = \Gamma_{\mathrm{G}} \tag{1}$$

$$\frac{\mathrm{d}}{\mathrm{d}z}\ (1-\alpha)\rho_{\mathrm{L}}u_{\mathrm{L}}\ = \Gamma_{\mathrm{L}} \tag{2}$$

– phase momentum equations

$$\frac{\mathrm{d}}{\mathrm{d}z}(\alpha\rho_{\mathrm{G}}u_{\mathrm{G}}^2) + \alpha\frac{\mathrm{d}P}{\mathrm{d}z} + \alpha\rho_{\mathrm{G}}\mathrm{g} = -F_{\mathrm{WL}} - F_{\mathrm{GL}} - F_{GI} \tag{3}$$

$$\frac{\mathrm{d}}{\mathrm{d}z}[(1-\alpha)\rho_{\mathrm{L}}u_{\mathrm{L}}^2 + (1-\alpha)\frac{\mathrm{d}P}{\mathrm{d}z} + (1-\alpha)\rho_{\mathrm{L}}\mathrm{g} = -F_{\mathrm{WL}} + F_{\mathrm{LG}} - F_{\mathrm{LI}} \tag{4}$$

– mixture energy equation

$$\frac{d}{\mathrm{d}z}\ (1-\alpha)\rho_{\mathrm{L}}u_{\mathrm{L}}H_{\mathrm{L}} + \alpha\rho u_{\mathrm{G}}H_{\mathrm{G}}\ = \frac{q_{\mathrm{w}}P_{\mathrm{h}}}{A} \tag{5}$$

Interfacial momentum transfer

The drag force, F_{LG}, is modeled according to Richter [23]:

$$F_{\mathrm{LG}} = \frac{3C_{\mathrm{FI}}}{D}\sqrt{\alpha}\rho_{\mathrm{G}}(u_{\mathrm{G}} - u_{\mathrm{L}})|u_{\mathrm{G}} - u_{\mathrm{L}}| + C'\rho_{\mathrm{G}}u_{\mathrm{G}}\alpha\frac{d}{\mathrm{d}z}(u_{\mathrm{G}} - u_{\mathrm{L}}) \tag{6}$$

where C′ is a virtual mass coefficient taken as: $C' = 0.5$ for bubbly flow, and $C' = 0$ for other flow regimes.

The interfacial friction factor C_{FI} is taken as:

$$\begin{aligned} C_{\mathrm{FI}} &= C_{\mathrm{D}}\sqrt{\alpha}(1-\alpha)^{-1.7}\frac{\rho_{\mathrm{L}}}{\rho_{\mathrm{G}}}\frac{D}{D_{\mathrm{B}}} \quad \text{for bubbly flow} \\ C_{\mathrm{FI}} &= 0.005[1+75(1-\alpha)] \quad \text{for annular flow} \end{aligned} \tag{7}$$

In the churn turbulent flow with a medium void fraction between the bubbly and annular flow, C_{FI} is interpolated linearly with the void fraction between the two values given in eq. (7).

The drag coefficient for a single bubble C_{D} in eq. (7) depends on the bubble Reynolds number, Re_{B}:

$$C_{\mathrm{D}} = \frac{24}{\mathrm{Re}_{\mathrm{B}}}(1 + 0.15\,\mathrm{Re}_{\mathrm{B}}^{0.687}) \qquad \mathrm{Re}_{\mathrm{B}} < 1000 \tag{8}$$

$$C_{\mathrm{D}} = 0.44 \quad \mathrm{Re}_{\mathrm{B}} \geq 1000 \tag{9}$$

where

$$\mathrm{Re}_{\mathrm{B}} = \frac{2\rho_{\mathrm{L}} R_{\mathrm{B}}(1-\alpha)\left|u_{\mathrm{G}} - u_{\mathrm{L}}\right|}{\mu_{\mathrm{L}}} \tag{10}$$

The interfacial momentum transfers F_{GI} and F_{LI} caused by the mass transfer can be determined from eqs. (3) and (4) while the liquid evaporates. The force associated with this velocity change is described by the following terms:

$$F_{\mathrm{LI}} = -(1-\eta)\Gamma_{\mathrm{L}}(u_{\mathrm{L}} - u_{\mathrm{G}}) \tag{11}$$

$$F_{\mathrm{GI}} = -\eta\Gamma_{\mathrm{G}}(u_{\mathrm{G}} - u_{\mathrm{L}}) \tag{12}$$

where η is the phase distribution factor, according to [18] η = 0.5 for bubbly flow and η = 0 in the other flow regime.

The wall-liquid friction F_{WL} is modeled by Chisholm's correlation [24] because it fits Baroczy's advanced empirical correlation curves quite well and takes into account the effect of mass flux on the friction pressure gradient. The correlation is expressed by the following set of equations:

$$F_{\mathrm{WL}} = 1 + (Y^2 - 1)[Bx^{(2-n)/2}(1-x)^{(2-n)/2} + x^{2-n}]\ \Delta P_{\mathrm{Lo}} \tag{13}$$

where ΔP_{Lo} is the single-phase friction pressure drop that would exist if the total mass flow of the two-phase mixture flowed as a single liquid phase and it is given by:

$$\Delta P_{\mathrm{Lo}} = \frac{4}{D} f_{\mathrm{Lo}} \frac{G^2}{2\rho_{\mathrm{L}}} \tag{14}$$

where n = 0.25 for the Blasius equation, and

$$Y = \left(\frac{\Delta P_{\mathrm{Go}}}{\Delta P_{\mathrm{Lo}}}\right)^{0.5} = \left(\frac{f_{\mathrm{Go}}}{f_{\mathrm{Lo}}}\right)^{0.5} \tag{15}$$

Coefficient B in eq. (13) is denoted as:

$$B = \frac{CY - 2^{2-n} + 2}{Y^2 - 1} \tag{16}$$

where

$$C = \frac{u_{\mathrm{G}}}{u_{\mathrm{L}}}\sqrt{\frac{\rho_{\mathrm{L}}}{\rho_{\mathrm{G}}}}\left(1 + \frac{u_{\mathrm{G}}^2}{u_{\mathrm{L}}^2}\frac{\rho_{\mathrm{G}}}{\rho_{\mathrm{L}}}\right) \tag{17}$$

and the true vapor mass quality is expressed as:

$$x = \frac{1}{1 + \frac{1-\alpha}{\alpha}\frac{\rho_L}{\rho_G}\frac{U_L}{U_G}} \tag{18}$$

Vapor generation rate

The heat transfer rate q_e due to evaporation can be modeled by the following equation:

$$q_e = C_2[q_w - C_1 h_{sp}(T_w - T_L)] \tag{19}$$

where C_1 and C_2 were estimated by Hainoun *et al.* [25]:

$$C_1 = 1 - \frac{\pi}{16}\frac{\alpha}{\alpha_{OSV}} \quad \text{for} \quad \alpha \le \frac{16\alpha_{OSV}}{\pi}$$
$$C_1 = 0 \quad \text{for} \quad \alpha > \frac{16\alpha_{OSV}}{\pi} \tag{20}$$

$$C_2 = \left(\frac{T_w - T_{sat}}{T_w - T_L}\right)^2 \tag{21}$$

where h_{sp} is the single liquid phase heat transfer coefficient given by:

$$h_{sp} = 0.023\frac{\lambda_L}{D}\mathrm{Re}_L^{0.8}\,\mathrm{Pr}_L^{0.4} \tag{22}$$

Re_L is the Reynolds number in the liquid phase expressed by:

$$\mathrm{Re}_L = \frac{GD(1-x)}{\mu_L} \tag{23}$$

The wall temperature T_w is calculated from:

$$q_w = h_{tp}(T_w - T_L) \tag{24}$$

Heat transfer coefficient in boiling two-phase flow is a function of many parameters such as mass flow rate and heat flux [26]. The method for expressing the forced convection boiling heat transfer coefficient h_{tp} is derived from Chen's well-known correlation [27]. The convective boiling heat transfer coefficient can be expressed as the arithmetic summation of the two-phase convection contribution h_{cv} and the boiling contribution h_{nb}:

$$h_{tp} = h_{cv} + h_{nb}$$
$$h_{cv} = Fh_{sp} \quad \text{and} \quad h_{nb} = Sh_{npb} \tag{25}$$

The factor F represents the acceleration effect of liquid due to vapor shear stress. The pool boiling heat transfer coefficient h_{npb} is computed for the same value of wall super heat as for forced convective boiling. The factor S represents the suppression of nucleate boiling due to the liquid flow.

Several correlations have been proposed for calculating F, S, and h_{npb}. In this paper we have used Chen's correlation [27]:

$$F = 1 \quad \text{for} \quad \frac{1}{Xtt} \le 0.1$$
$$F = 2.35\left(\frac{1}{Xtt} - 0.213\right)^{0.736} \quad \text{for} \quad \frac{1}{Xtt} > 0.1 \tag{26}$$

The Lockhart-Martinelli parameter is expressed by:

$$\frac{1}{Xtt} = \left(\frac{\rho_L}{\rho_g}\right)^{0.5}\left(\frac{\mu_g}{\mu_L}\right)^{0.1}\left(\frac{x}{1-x}\right)^{0.9} \tag{27}$$

$$S = \frac{1}{1 + 2.35\cdot 10^{-6}\,\mathrm{Re}_{tp}^{1.17}} \tag{28}$$

$$h_{npb} = 0.00122\frac{\mu_L^{0.79} C_{PL}^{0.45} \rho_L^{0.49}}{\sigma^{0.5}\mu_L^{0.29} h_{fg}^{0.24} \rho_g^{0.24}} \Delta T_{sat}^{0.24} \Delta P_{sat}^{0.75} \tag{29}$$

where Re_{tp} is the two-phase Reynolds number expressed by:

$$\mathrm{Re}_{tp} = F^{1.25}\frac{G(1-x)D}{\mu_L} \tag{30}$$

$$\Delta T_{sat} = T_w - T_{sat} \quad \text{and} \quad \Delta P_{sat} = P_{sat}(T_w) - P_{sat}(T_{sat}) \tag{31}$$

The vapor generation rate is given by the following expression:

$$\Gamma_G = -\Gamma_L = \frac{q_e}{h_{fg} + C_{PL}\Delta T_{sat}} \tag{32}$$

Numerical resolution

Equations 1 to 5, which govern the evaporation of refrigerant flowing in the vertical tube, have five unknown parameters, namely α, u_L, u_G, P, and h_L. To solve this set of equations numerically, the tube was divided into infinitesimal sections. The heat flux, q_w, and the following inlet operating conditions for the refrigerant were considered:

– inlet saturation pressure or inlet mixture temperature,
– mixture mass flow rate, and
– inlet flow quality.

The equations were solved using the fourth order Runge-Kutta method and for operated conditions illustrates in tab. 1.

The mixture is assumed to be saturated in inlet of bubble pump tube. The correlation between P-T-x, for the liquid phases, is given by Bourseau *et al.* [28]. The density of the liquid mixture is calculated according to Tiliner-Roth *et al.* [29]. The vapor density and the enthalpy are only depended on the pressure:

$$\rho_G = \rho_{G,\,sat}\,(P)$$

$$H_G = h_{G,\,sat}\,(P)$$

Table 1. Operating conditions considered for simulation

Parameters		Values
Heat flux, q	kWm^{-2}	1-30
Tube diameters, D	mm	4, 6, 8, 10
Mass flow rate, G	$kgm^{-2}s^{-1}$	50
Tube length, L	m	1.000
Ammonia fraction in inlet solution, X_{in}	–	0.3, 0.4, 0.5, 0.6
Inlet pressure, P_{in}	bar	12, 15, 17, 18

Model validations

To validate the two-fluid model presented a comparison of the calculated values for void fraction *vs*. vapor quality using this model was compared with those obtained from three other models: homogenous model, Rouhani and Axlesson drift model [30] and Zivi annular model [31].

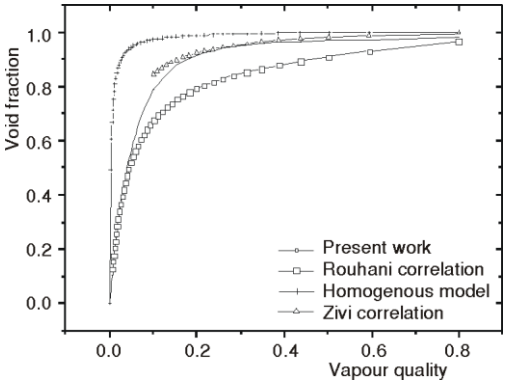

Figure 2. Comparison of void fraction simulated with other models

It can be observed in fig. 2 that the numerical values achieved in the present work show similar trend to the results of other models. For void fractions lower than 0.6 there is a great similarity between the calculated values using Rouhani and Axelsson's correlation and our results, being the absolute deviation between 1.3 and 8.0%. For void fractions above 0.6, the absolute deviation is larger and can reach 17.0%. Regarding the Zivi's model, which is applicable for annular flow regime ($\alpha > 0.8$), it gives values very close to our simulation results. The absolute deviation of this model does not exceed 5.5% and may decrease to 0.37%. The difference deviation between the values from the homogenous model and our numerical results is significant. This is due to the fact that in the homogenous model it is assumed that both liquid and vapour phases are flowing with the same velocity, which is not the case in our model as well as in practice.

Simulated results

Liquid velocity

The influence of heat input in the different operating conditions on the outlet liquid velocity is shown in fig 4. The outlet liquid velocity presents the same behavior in the three figures. It increases, reached a maximum and then decrease. This behavior is explained by the change of flow regime of slug to churn. Using a higher heat input results in increased desorption *i. e*., a reduction in refrigerant concentration at the tube exit, resulting, in turn, in a higher gas volume fraction and in increasing velocities and temperatures of the gas and liquid phases [10].

The influence of the operating pressure on liquid velocity is shown in fig. 3(a). For any fixed inlet pressure value, the outlet liquid velocity increases with increasing heat flux, reaches a maximum, then decreases. Inversely, for a fixed heat value (namely for all $q_w \geq 5$ kW/m^2), the outlet liquid velocity increases with the operating pressure. This is explained by the increasing of the vapor density, resulting, in turn, a reduction of the vapor velocity.

Figure 3(b) presents the outlet liquid velocity evolution *vs.* heat flux for five different tube diameters at a constant operating pressure of 15 bar and ammonia fraction in inlet solution of 0.4. For tube diameters, namely, 4 and 6 mm, the liquid velocity increases, reaches a maximum and then decreases. But it increases for a diameter exceeds 8 mm. The value of heat flux that corresponds to the maximum liquid velocity depends on tube diameter. The heat flux required to produce the maximum liquid velocity is about 15 kW/m^2 for 4 mm and 25 kW/m^2 for a 6 mm tube diameter. While for 8, 10, and 12 mm tube diameter, maximum outlet velocity was not achieved for the range of operating heat input. As the tube diameter increases, the frictional pressure drop decreases and the occurrence of the maximum liquid velocity is shifted to the right side, *i. e.*, to the higher heat input side.

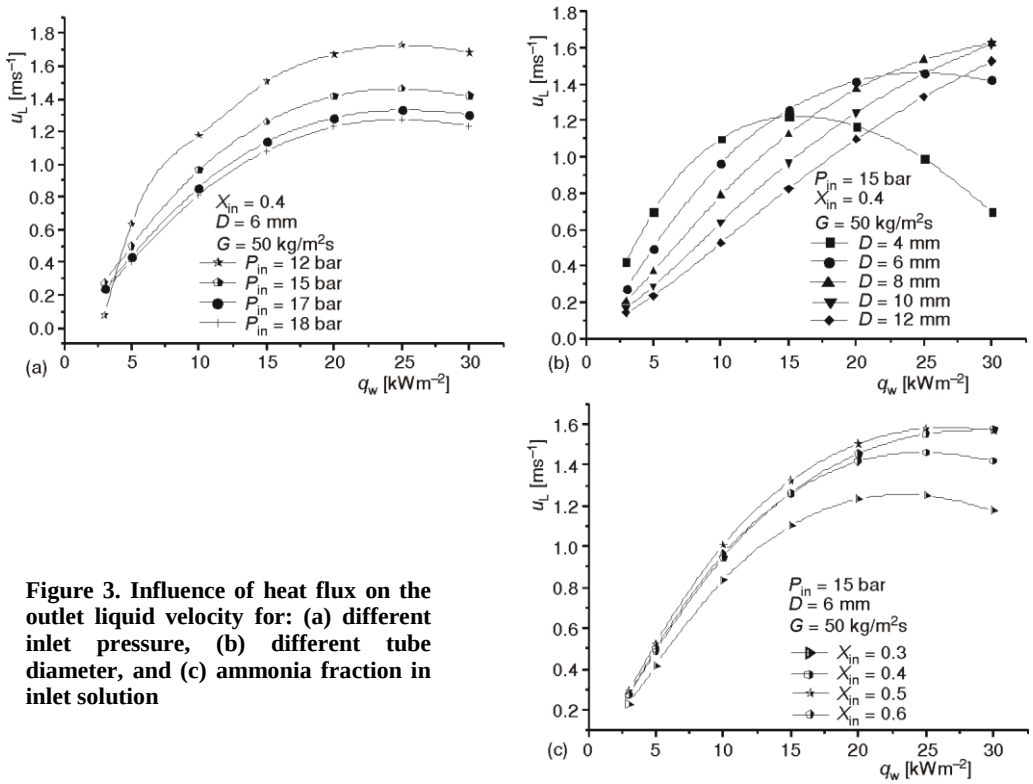

Figure 3. Influence of heat flux on the outlet liquid velocity for: (a) different inlet pressure, (b) different tube diameter, and (c) ammonia fraction in inlet solution

The variation of the outlet liquid velocity with the heat input for a constant tube diameter of 6 mm, constant inlet pressure (P_{in} = 15 bar) and different ammonia fraction in inlet solution is shown in fig. 3(c). As can be seen, for all ammonia fractions, the maximum liquid velocity is obtained for heat flux about 25 kW/m^2. The outlet liquid velocity increases with ammonia mass fraction for any fixed heat flux. This is due to the fact, the saturation temperature increases with the ammonia fraction.

Vapor velocity

The effect of heat flux on vapor velocity is presented in fig. 4. They show a linear increasing of outlet vapor velocity with the heat flux. The variation of the outlet vapor velocity *vs.* heat flux presents for all studied conditions, similar shapes. The outlet vapor velocity decreases if tube diameter increases, fig. 4(c). This is related to the increase in the hydraulic load in tube. Same behavior is shows for different inlet pressure and different ammonia fraction, figs. 4(a) and 4(b).

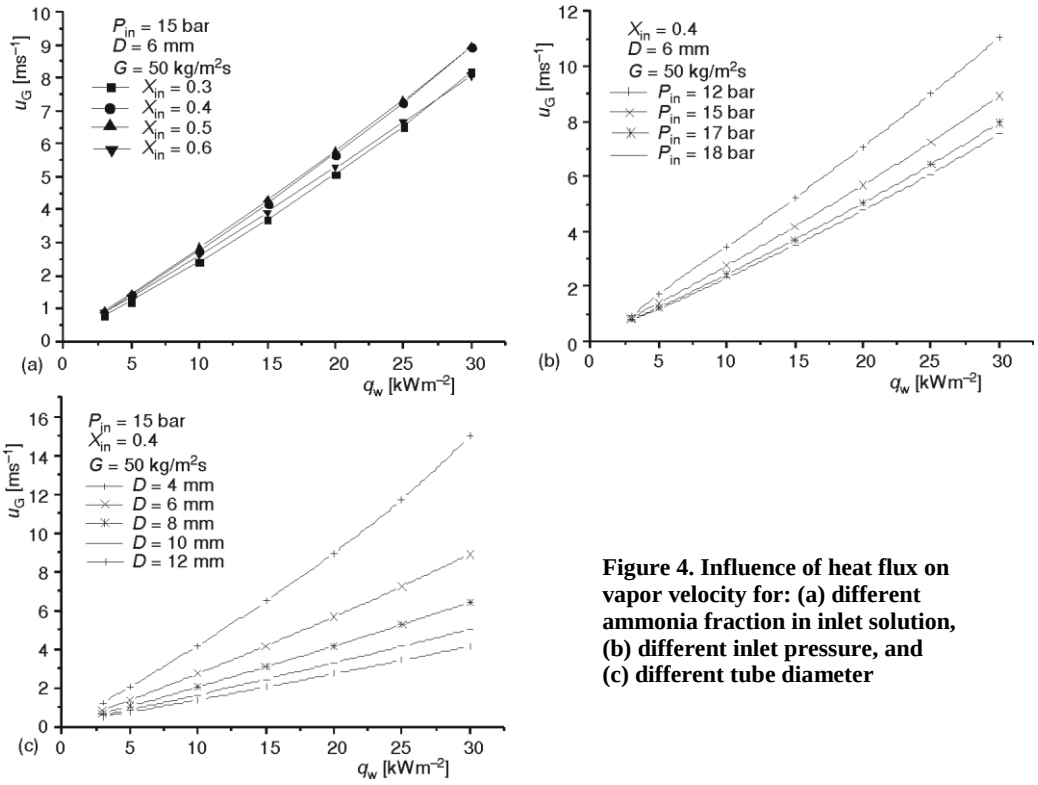

Figure 4. Influence of heat flux on vapor velocity for: (a) different ammonia fraction in inlet solution, (b) different inlet pressure, and (c) different tube diameter

Pumping ratio

The pumping ratio R_p is the ratio of liquid velocity (u_L) to vapor velocity (u_G). The variation of the pumping ratio with the heat flux for different inlet pressure values is plotted in fig. 5(a), at different ammonia fraction values is given by fig. 5(b) and for different tube diameters, is shown in fig. 5(c). From theses curves, the general behavior of the pumping ratio with respect to the heat flux seems similar. The evolution of pumping ratio *vs.* heat input at different operating conditions presents a maximum. This which gives the optimal value of heat flux input. Indeed, the optimal value of heat flux is the value that corresponds to a maximum pumping ratio.

Figures 5(a) and 5(b), show a low dependence of pumping ratio with inlet pressure and ammonia fraction. For these parameters, the maximum pumping ratio is obtained for a

heat flux localized between 5 and 10 kW/m^2. However, the variation of the tube diameter has a significantly affects on the pumping ratio. Figure 5(c) shows that for the small diameters (D = = 4 and 6 mm), the maximum pumping rate is reached at a lower heat flux, ranging between 3 and 5 kW/m^2. It increases when the tube diameter increases (10, 15, and 17.5 kW/m^2 for D = = 8, 10, and 12 mm, respectively). However Pfaff *et al*. [7] showed that the pumping ratio is independent of heat input for a rung tube diameter between 10 and 18 mm, which is due to the fact, there's no transition flow regime for the tubes diameters studied. They showed an increase with driving head, a result indicates a transition regime.

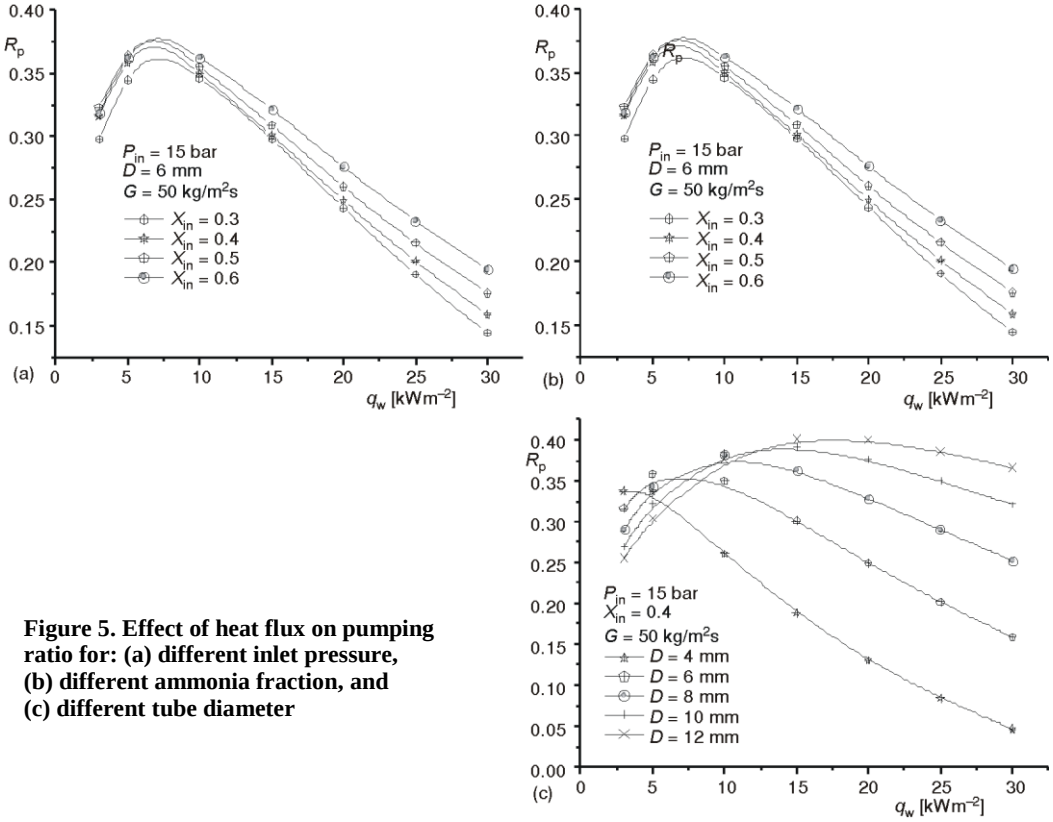

Figure 5. Effect of heat flux on pumping ratio for: (a) different inlet pressure, (b) different ammonia fraction, and (c) different tube diameter

As can be see, a certain minimum heat input denoted ($Q_{min.}$) is required for the pump to operate. Before $Q_{min.}$ was reached, the driving force was not sufficient for pumping action. The mixing ammonia-water boiled off but the solution only oscillated in the pump without being conveyed to the boiler [7]. It is important to notice that for most significant diameters, the range of heat flux corresponding to maximum pumping ratio is broader. In fact, pumping ratio is slightly influenced by moderate variation of heat flux.

Conclusions

In the present work, the two-fluid model was used for the two-phase flow region of ammonia-water mixing, considering the hydrodynamic non-equilibrium between the liquid and vapor phases. On the basis of the numerical simulations, a detailed description of the flow

characteristics was obtained. The influence of the heat input and operating conditions on the flow characteristics was examined. The following conclusions are deduced.

- Vapor velocity varies linearly with heat flux, whereas the liquid velocity and the pumping rate variations present a maximum values that depend on operating conditions. Inlet pressure and ammonia fraction does a stately influence on the parameters flow.
- The bubble pump optimum functioning are defined when the pumping ratio is maximal. The results shows, the value of heat flux corresponding to the optimal functioning are more influenced by tube diameter (3 kW/m^2 for a 4 mm of tube diameter and 5, 10, 13, and 17 kW/m^2, respectively for 6, 8, 10, and 12 mm of tube diameter). It increase with tube diameter, but it's weak influenced by varying of inlet pressure or ammonia fraction.
- It is important to notice that for most significant diameters, the range of heat flux corresponding to maximum pumping ratio is broader. In fact, pumping ratio is slightly influenced by moderate variation of heat flux.

Nomenclature

A – tube cross-section area, [m^2]
C_1 – the portion of the heating surface not covered by bubbles, [m^2]
C_P – specific heat, [Jkg^{-1}°C^{-1}]
D – tube diameter, [mm]
F – convective boiling factor, [–]
f_{Lo} – fraction factor, [–]
F_{GI} – interfacial force for the vapor due to – the mass exchange, [Nm^{-3}]
F_{LG} – interfacial force between the two phases, [Nm^{-3}]
F_{LI} – interfacial force for the liquid due to the – mass exchange, [Nm^{-3}]
F_{WG} – force between the wall surface and the vapor, [Nm^{-3}]
F_{WL} – force between the wall surface and the – liquid, [Nm^{-3}]
G – mass flux flowing in the tube, [kgm^{-2}s^{-1}]
g – gravity acceleration, [ms^{-2}]
H – enthalpy, [Jkg^{-1}]
h – heat transfer coefficient, [Wm^{-2}K^{-1}]
h_{fg} – evaporation heat from the liquid to the vapor, [Jkg^{-1}]
L – length, [m]
P – pressure, [Pa]
P_h – heating perimeter of the channel, [m]
Pr – Prandlt number (= $Cp\mu/\lambda$), [–]
ΔP – pressure drop, [Pa]
q – total wall heat flux, [Wm^{-2}]
q_v – heat flux component for generating the – vapor on the wall surface, [Wm^{-2}]
R_B – bubble radius, [m]
Re – Reynolds number (= UD/μ), [–]
T – temperature, [K]
u – velocity, [ms^{-1}]
x – vapor quality, [–]
z – axial location along the flow direction, [m]

Greek symbols

α – void fraction, [–]
Γ – vapor or liquid generation rate per unit mixture volume, [kgm^{-3}s^{-1}]
μ – dynamic viscosity, [Pas]
ρ – density,[kgm^{-3}]
σ – surface tension, [Nm^{-1}]

Subscripts

B – bubble
CV – convective
G – vapor
Go – vapor only
H – hydraulic
In – inlet
L – liquid
Lo – liquid only
nb – nucleate boiling
npb – nucleate pool boiling
OSV – onset of significant void
sat – saturation condition
tp – tow phase
w – wall

References

[1] Koyfman, A., *et al.*, An Experimental Investigation of Bubble Pump Performance for Diffusion Absorption Refrigeration System with Organic Working Fluids, *Applied Thermal Engineering, 23* (2003), 15, pp. 1881-1894

[2] Srikhirin, P., Aphornratana, S., Investigation of a Diffusion Absorption Refrigerator, *Applied Thermal Engineering, 22* (2002), 11, pp. 1181-1193
[3] Vicatos, G., Bennett, A., Multiple Lift Tube Pumps Boost Refrigeration Capacity in Absorption Plants, *Journal of Energy in Southern Africa, 18* (2007), 3, pp. 49-57
[4] Nicklin, D. J., The Air-Lift Pump: Theory and Optimization, *Transactions of the Institute of Chemical Engineers, 41* (1963), pp. 29-38
[5] Lister, G. D. S., The Design and Evaluation of a Pumping System for a Three Fluid Absorption Refrigeration Plant, B. Sc. Thesis, University of Cape Town, Cape Town, South Africa, 1996
[6] Jeong, S., Lee, S. K., Koo, K. K., Pumping Characteristics of a Thermosyphon Applied for Absorption Refrigerators with Working Pair of Li/Br, *Applied Thermal Engineering, 18* (1998), 18, pp. 1309-1323
[7] Pfaff, M., *et al*., Studies on Bubble Pump for a Water-Lithium Bromide Vapor Absorption Refrigeration, *International Journal of Refrigeration, 21* (1998), 6, pp. 452-462
[8] Delano, A. D., Design Analysis of the Einstein Refrigeration Cycle, Ph. D. thesis, Georgia Institute of Technology, Atlanta, Geo., USA, 1998
[9] White, S. J., Bubble Pump Design and Performance, M. Sc. thesis, Georgia Institute of Technology, Atlanta, Geo., USA, 2001
[10] Levy, A., Koyfman, A., Jelinek, M., Flow Boiling of Organic Binary Mixtures, *Int. J. Multiphase Flow, 32* (2006), 10, pp. 1300-1310
[11] Jakob, U., *et al*., Simulation and Experimental Investigation in to Diffusion Absorption Cooling Machines for Air-Conditioning Applications, *Applied Thermal Engineering, 28* (2008), 10, pp. 1138-1150
[12] Zohar, A., *et al*., The Influence of the Generator and Bubble Pump Configuration on the Performance of Diffusion Absorption Refrigeration (DAR) System, *International Journal of Refrigeration, 31* (2008), 6, pp. 962-969
[13] Ben Ezzine, N. B., Garma, R., Bourouis, M., Bellagi, A., Experimental Studies on Bubble Pump Operated Diffusion Absorption Machine Based on Light Hydrocarbons for Solar Cooling, *Renewable Energy, 35* (2010), 2, pp. 464-470
[14] Beattie, D. R. H., Whalley, P. B., A Simple Two-Phase Frictional Pressure Drop Calculation Method, *Int. J. Multiphase Flow, 8* (1982), 1, pp. 83-87
[15] Zuber, N., Findlay, J., Average Volumetric Concentration in Two-Phase Flow Systems, *J. Heat Transfer, 87* (1965), pp. 453-468
[16] Yang, L., Zhang, C. L., Two-Fluid Model of Refrigerant Two-Phase Flow through Short Tube Orifice, *Int. J. Refrigeration, 28* (2005), 3, pp. 419-427
[17] Seixlak, A. L., Barbazelli, M. R., Numerical Analysis of Refrigerant Flow Along Non-Adiabatic Capillary Tubes Using a Two-Fluid Model, *App. Ther. Science, 29* (2009), 2, pp. 523-531
[18] Xu, J. L., Wong, T. N., Huang, X. Y., Two-Fluid Modeling for Low-Pressure Subcooled Flow Boiling, *Int. J. Heat and Mass Transfer, 49* (2006), 2, pp 377-386
[19] Platen, B. C. V., Munters, C. G., Refrigerator, U. S. Patent No. 1: 685-764, 1928
[20] Chaouachi, B., Gabsi, S., Design and Simulation of an Absorption Diffusion Solar Refrigeration Unit, *Am. J. Applied Sciences, 4* (2007), 2, pp. 85-88
[21] Gutierrez, F., Behavior of a Household Absorption Diffusion Refrigerator Adapted to Autonomous Solar Operation, *Solar Energy, 40* (1988), 1, pp. 17-23
[22] Ishii, M., Mishima, K., Two-Fluid Model and Hydrodynamic Constitutive Relations, *Nuclear Engineering Design, 82* (1984), 2, pp. 107-126
[23] Richter, H. J., Separated Two-Phase Flow Model, Application to Critical Two Phase Flow, *International Journal of Multiphase Flow, 9* (1983), 5, pp. 511-530
[24] Chisholm, D., Pressure Gradient Due to Friction During the Flow of Evaporating Two Phase Mixtures in Smooth Tubes and Channe, *Int. J. Heat Mass Transfer, 16* (1973), 2, pp. 347-358
[25] Hainoun, A., Hicken, E., Wolters, J., Modelling of Void Formation in the Subcooled Boiling Regime in the ATHLET Code to Simulate Flow Instability for Research Reactors, *Nuclear Engineering Design, 16* (1996), pp. 7175-7191
[26] Balakrishna, R., Dhasan, M. L.,Rajagopal, S., Flow Boiling Heat Transfer Coefficient of R-134a/A-290/R-600a Mixture in a Smooth Horizontal Tube, *Thermal Science, 12* (2008), 3, pp. 33-44
[27] Chen, J. C., Correlation for Boiling Heat Transfer to Saturated Fluids in Convective Flow, Industrial Engineering Chemical Process Design and Development, 5 (1966), 13, pp. 322-329
[28] Bourseau, P., Bugarel, R., Absorption-Diffusion Machines; Comparison of the Performances of NH_3–H_2O and NH_3– NaSCN, *Int. J. Refrigeration, 9* (1986), 4, pp. 206-214

[29] Tiliner-Roth, R., Friend, D. G., Survey and Assessment of Available Measurements on Thermodynamic Properties of the Mixture (Water + Ammonia), *J. Phys. Chem. Ref. Data, 27* (1988), 1, pp. 45-61
[30] Rouhani, Z., Axelsson, E., Calculation of Volume Void Fraction in the Subcooled and Quality Region, *Int. J. Heat Mass Transfer, 13* (1970), 2, pp. 383-393
[31] Zivi, S. M., Estimation of Steady-State Steam Void Fraction by Means of Principle of Minimum Entropy Production, *Trans. ASME. J. Heat Transfer, 86* (1964), pp. 247-252

Paper submitted: June 1, 2010
Paper revised: January 6, 2011
Paper accepted: January 23, 2011